Topside Ionosphere Sounding From the CHAMP, GRACE, and GRACE-FO Missions

Schreiter, Lucas; Stolle, Claudia; Rauberg, Jan; Kervalishvili, Guram; van den Ijssel, Jose; Arnold, Daniel; Xiong, Chao; Callegare, Andyara

DOI
10.1029/2022RS007552

Publication date
2023

Document Version
Final published version

Published in
Radio Science

Citation (APA)
Schreiter, L., Stolle, C., Rauberg, J., Kervalishvili, G., van den Ijssel, J., Arnold, D., Xiong, C., & Callegare, A. (2023). Topside Ionosphere Sounding From the CHAMP, GRACE, and GRACE-FO Missions. *Radio Science*, *58*(3), Article e2022RS007552. https://doi.org/10.1029/2022RS007552

Radio Science

RESEARCH ARTICLE
10.1029/2022RS007552

Topside Ionosphere Sounding From the CHAMP, GRACE, and GRACE-FO Missions

Lucas Schreiter[1], Claudia Stolle[2], Jan Rauberg[1], Guram Kervalishvili[1], Jose van den Ijssel[3], Daniel Arnold[4], Chao Xiong[5], and Andyara Callegare[1,6]

[1]GFZ German Research Centre for Geosciences, Potsdam, Germany, [2]Leibniz Institute for Atmospheric Physics at the University of Rostock, Kühlungsborn, Germany, [3]Faculty of Aerospace Engineering, Delft University of Technology, Delft, The Netherlands, [4]Astronomical Institute, University of Bern, Bern, Switzerland, [5]Wuhan University, Wuhan, China, [6]University of Potsdam, Potsdam, Germany

Abstract Satellites in Low Earth Orbit (LEO) are essential for sounding the topside ionosphere. In this work, we present and validate a data set of Total Electron Content (TEC) and in situ electron density observations from the Gravity Recovery And Climate Experiment (GRACE) and GRACE-Follow-On missions as well as a TEC data set from the CHAllenging Minisatellite Payload mission. Concerning TEC, special emphasis is put to ensure optimal consistency to the already existing Swarm and Gravity field and steady-state ocean circulation explorer (GOCE) TEC data sets. The newly processed satellite missions allow covering two full solar cycles with LEO slant TEC. Furthermore, the twin satellite missions GRACE and GRACE-FO equipped with inter-satellite K-band ranging allows to derive the horizontal TEC and, due to the small inter-satellite distance of the satellite pairs, an approximation for local electron density. However, the derived value of electron density is relative and requires calibration using external information. In this work, the calibration is performed using the IRI-2016 model. Radar observations, as well as in situ electron density observations available from Swarm B Langmuir probes, are used for validation. Conjunctions between satellites are used to validate the TEC time series. The newly derived data set is shown to be highly consistent with the already existing data sets with standard deviations below 3 TECU for TEC (even 1 TECU was reached for low solar flux) and an offset below 7×10^{10} m^{-3} with a standard deviation near 1×10^{11} m^{-3} for the electron density.

Key Points:

- Two full solar cycles are covered by Low Earth Orbit (LEO) Global Positioning System (GPS) Total Electron Content (TEC) observations by adding CHAllenging Minisatellite Payload (CHAMP), Gravity Recovery And Climate Experiment (GRACE) and GRACE-Follow-On (FO) to support Swarm
- Local electron density is approximated using inter-satellite K-band ranging of the GRACE satellites
- LEO GPS TEC from the missions considered and GRACE(-FO) electron density observations are highly consistent to Swarm observations

Correspondence to:
L. Schreiter,
schreit@gfz-ptosdam.de

Citation:
Schreiter, L., Stolle, C., Rauberg, J., Kervalishvili, G., van den Ijssel, J., Arnold, D., et al. (2023). Topside ionosphere sounding from the CHAMP, GRACE, and GRACE-FO missions. *Radio Science*, *58*, e2022RS007552. https://doi.org/10.1029/2022RS007552

Received 30 JUN 2022
Accepted 25 FEB 2023

1. Introduction

The ionosphere contains ionized gas. The distribution of the ionized particles is essential to describe the ionosphere. Total electron content (TEC), the integrated electron density along the propagation path, is modeled on a routine basis using the international Global Navigation Satellite System (GNSS) service (IGS) ground station network (Schaer, 2011) The distribution of the ground stations is however unequal. Besides, several key parameters of the ionosphere, such as the electron densities peak height, and scale height, cannot be assessed using ground-based GNSS stations. Ionosondes can be used for estimating ionospheric profiles, however, by design, they are only capable of measuring up to the F2 peak and the topside is essentially invisible. Topside sounders, that could provide topside profiles, like the Isis or Alouette missions between 1962 and 1990, were used, for example, to develop the International Reference Ionosphere (IRI) model (Bilitza & Williamson, 2000) but are not operational anymore. Incoherent scatter radars are capable to measure across the F2 peak, however, the signal degrades rapidly above about 400 km, and the number of available stations is rather limited. LEO satellites remain the only means to access the topside electron content. LEO satellites can be equipped with different instruments to observe the upper ionosphere. For example, TEC can be derived form radars onboard altimetry missions, slant TEC measurements from using high-low satellite to satellite tracking (SST, e.g., GNSS) or low-low SST (e.g., K-band Ranging), or in situ electron density from Langmuir probes (LP). If two LEO satellites are sufficiently close, low-low SST may be also used to approximate the local electron density. An extended database of TEC and electron density measurements is especially useful to improve the topside model of the ionosphere for example, of IRI, which was demonstrated recently by Bilitza and Xiong (2021). However, it is important that new data sets as presented here are consistent with existing data sets from already available satellite missions, for example, electron densities and TEC from the Swarm satellite mission.

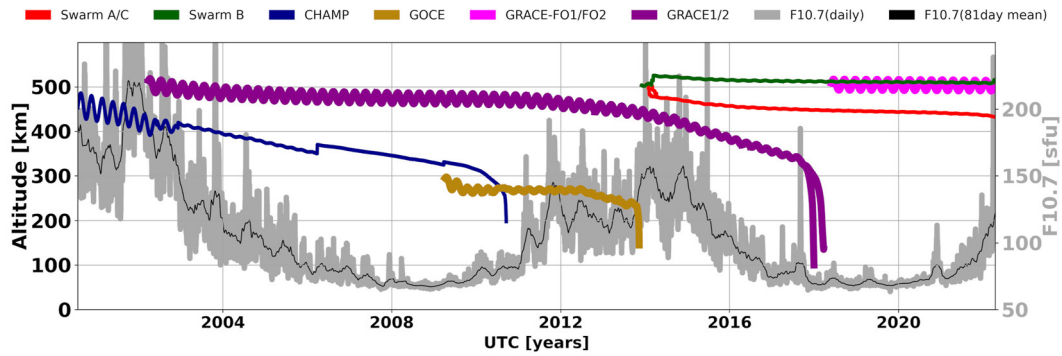

Figure 1. Altitude development of CHAllenging Minisatellite Payload, Gravity Recovery And Climate Experiment, and GRACE-FO together with Swarm and GOCE in combination with the F10.7 solar flux index.

This work presents results from the Topside Ionosphere from LEO Radio Observations (TIRO) project, which has been funded by the Swarm Data Innovation and Science Cluster (DISC) framework of ESA. It aims at extending the existing Swarm database of topside Global Positioning System (GPS) derived TEC measurements and in situ electron density measurements to cover different altitudes, local times, and allow long term studies. GPS TEC from Swarm and GOCE (Drinkwater et al., 2006) are available (DISC, 2017; Kervalishvili et al., 2019), in this work GPS TEC for CHAllenging Minisatellite Payload (CHAMP, Reigber et al., 1999), and the twin satellite missions Gravity Recovery And Climate Experiment (GRACE, Tapley et al., 2004) and GRACE Follow-On (FO) will be added. In contrast to Swarm, GRACE and GRACE-FO are not equipped with LP to measure the in situ electron density. The key mission instrument onboard GRACE and GRACE-FO is the KBR. This system is designed to measure the relative change of the inter-satellite distance and can be also used to measure the relative inter-satellite TEC (Case et al., 2010). The short distance between the satellites of only about 200 km allows the transformation of inter-satellite TEC to an estimate of the mean electron density between the satellites. Absolute calibration of the inter-satellite electron density is performed using the IRI-2016 (Bilitza, 2018). The orbits of the considered satellites are near polar, with inclinations of 87° (CHAMP) and 89° (GRACE and GRACE-FO). Their initial altitudes were around 500 km and orbits were designed to drift slowly in local time (see Figures 1 and 2). The satellites are at a nominal distance of 200 km. The inter-satellite distance is subject to gravitational acceleration. Long-time variation in the inter-satellite distance is shown in Figure 3.

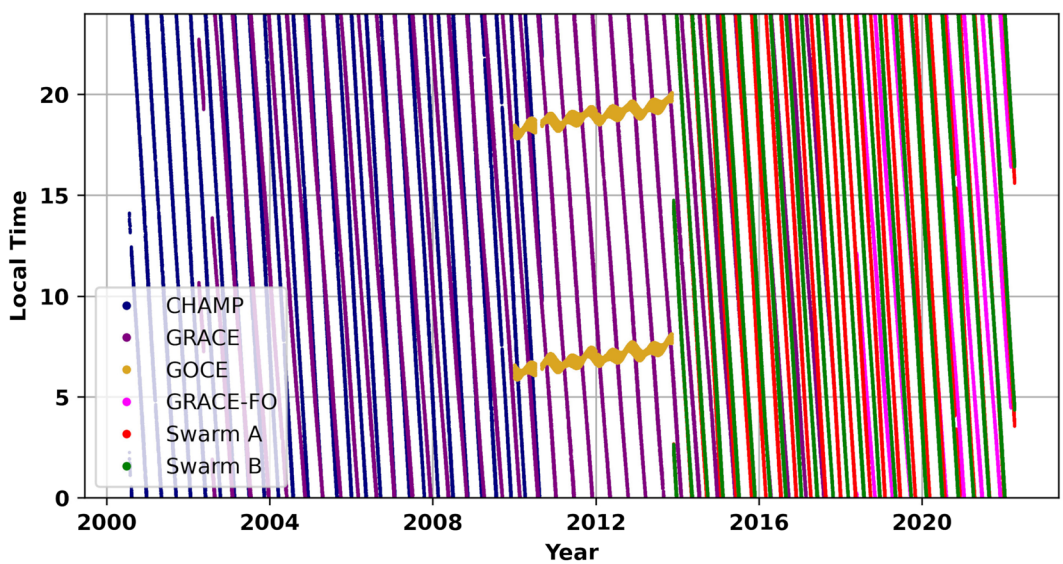

Figure 2. Local time evaluations of CHAllenging Minisatellite Payload, Gravity Recovery And Climate Experiment, and GRACE-FO together with Swarm and GOCE.

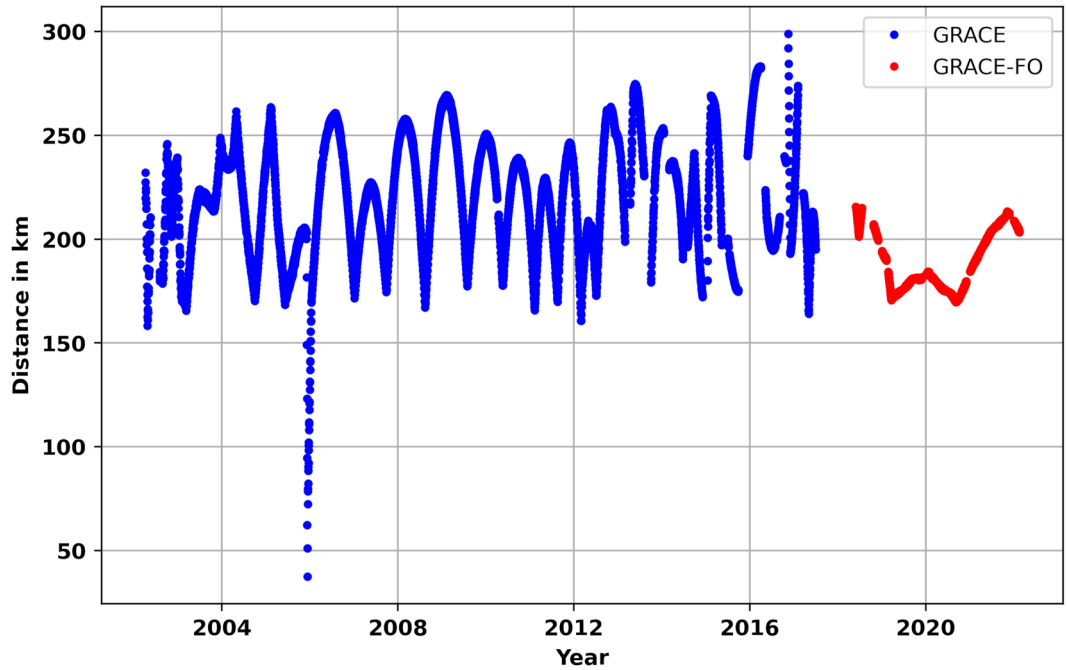

Figure 3. Inter-satellite distance for the twin satellite missions Gravity Recovery And Climate Experiment and GRACE-FO.

Local electron density derived from GRACE KBR radio links has earlier been published by Xiong et al. (2021) until April 2015. Its value for space science has been proven, for example, by Xiong et al. (2010), Bilitza and Xiong (2021), Lei et al. (2014), or Smirnov et al. (2021). The approach presented in this work has been revised, for example, a calibration against the IRI model instead against radars is proposed for sake of continuity, and variable distances between the two GRACE satellites are accounted for.

2. Methods

2.1. TEC From GNSS

Free electrons on a polarized electromagnetic wave, such as GNSS signals, cause a phase advance and a code delay, which is to first-order proportional to $1/f^2 \int Nedl$, where f is the frequency and Ne the electron density in m^{-3}. The integral is evaluated along the line of sight. In the case of GPS and KBR two carrier frequencies (GPS: 1575.42 and 1227.60 MHz, KBR: 24 and 32 GHz) are used, which allows to either mitigate the impact of free electrons on the range measurement, or isolate the integrated electron density to receive the slant TEC. Higher-order ionospheric terms (see e.g., Fritsche et al., 2005) may be neglected for TEC estimation, as their impact remains sufficiently small. To first order the phase measurement on frequency $i = 1, 2$ can be described as

$$\phi_{Li} = \tilde{\varrho} + n_i \lambda_i - \frac{q}{f_i^2}, \tag{1}$$

with $\tilde{\varrho}$ containing the slant range, tropospheric delay, and clock corrections. The number of phase ambiguities is n_i with wavelength λ_i, the fist order ionospheric term is q and f_i is the carrier frequency. For code observations the following expression is obtained:

$$\phi_{Pi} = \varrho + \frac{q}{f_i^2} \tag{2}$$

The first order term $\left(q/f_i^2\right)$, where

$$q = \frac{1}{2} \int_{LEO}^{GPS} f_p^2 dl \frac{\mathrm{m}^3}{\mathrm{s}^2} = 40.3 \int_{LEO}^{GPS} N_e dl \cdot \frac{\mathrm{m}^3}{\mathrm{s}^2} = 40.3 \cdot TEC \frac{\mathrm{m}^3}{\mathrm{s}^2} \tag{3}$$

can be eliminated using the ionosphere-free linear combination or isolated using the geometry-free linear combination (see e.g., Dach et al., 2015). The latter reads for code measurements

$$P_{gf} = P_2 - P_1 \tag{4}$$

and for phase measurements

$$L_{gf} = L_1 - L_2. \tag{5}$$

Note the opposite sign caused by the different signs of the ionospheric terms for code and phase.

Phase measurements are typically much less affected by noise compared to code observations (in the order of 1 mm compared to 1 m) but they contain the generally unknown phase ambiguity. This ambiguity is not present in code measurements, therefore a commonly used approach is to estimate the ambiguity or absolute offset of the geometry-free linear combination of phase observations using the code observations (DISC, 2017; Yue et al., 2011). This approach requires accounting for code biases. In the case of the geometry-free linear combination of code measurements, the essential biases are the GPS satellite-specific differential code biases (DCB) (Schaer, 2011) (available at IGS and CODE), the receiver specific DCB, and the near field multi-path. The latter both have to be estimated as follows. Near-field multi-path maps are estimated using the linear combinations (Montenbruck & Kroes, 2003)

$$M_{P1} + \psi_{P1} \approx \phi_{P1} - \frac{2}{f_1^2 - f_2^2}\left(f_1^2\phi_{L2} - f_2^2\phi_{L1}\right) - \phi_{L1} - B_{P1}, \tag{6}$$

$$M_{P2} + \psi_{P2} \approx \phi_{P2} - \frac{2}{f_1^2 - f_2^2}\left(f_1^2\phi_{L2} - f_2^2\phi_{L1}\right) - \phi_{L2} - B_{P2}. \tag{7}$$

where B is a bias term, assumed to be constant as long as no cycle slips or phase breaks occur and ψ is the code noise (assumed to be Gaussian with zero mean). All satellites considered in this paper have a static geometry (e.g., no rotating solar panels). Dependencies on the solar beta angle can therefore be neglected. The multi-path values are binned in 1° elevation and azimuth and averaged daily. The multi-path pattern is well known to be affected by the operational mode of the occultation antenna. This was observed for example, by Montenbruck and Kroes (2003). Due to the daily stacking, the separation between occultation antenna on and off is nearly always automatically taken into account.

Using the multi-path corrected code measurements the leveling of the phase observations can be conducted by taking the GPS DCB into account. To estimate the receiver-specific P1-P2 DCB an elevation-dependent mapping function is used following the approach from Yue et al. (2011). Here we use the so-called slab layer mapping function developed by Foelsche and Kirchengast (2002) which is especially suited for LEO satellites. The thickness of the slab layer H_{shell} is assumed to be 400 km. With the radius of the satellite orbit from the Earth center (R_{sat}), the elevation (ϵ) depending mapping function is formulated as

$$M(\epsilon) = \frac{H_{shell}}{R_{sat} + H_{shell}}\left\{\cos\left(\sin^{-1}(r \cdot \cos(\epsilon))\right) - r\sin(\epsilon)\right\}^{-1} \tag{8}$$

with

$$r = \frac{R_{sat}}{R_{sat} + H_{shell}}. \tag{9}$$

The differential $P_1 - P_2$ receiver bias b_{rec} is estimated using simultaneously observed relative slant TEC measurements ($rsTEC$) with elevation ϵ. The equation

$$M(\epsilon_1) \cdot (rsTEC_1 + b_{rec}) = M(\epsilon_2) \cdot (rsTEC_2 + b_{rec}) \tag{10}$$

should be satisfied. The differential P1–P2 receiver bias b_{rec} is estimated in a least-squares approach using suitable pairs at ionospheric quiet conditions in mid latitudes below 50° with $rsTEC$ values that are less than 10 TECU above the minimum rsTEC observed on the specific day to avoid highly variable regions of the ionosphere. Additionally, an elevation mask of 20° is used to mitigate the impact of mapping errors from low elevations. This

approach is also used in Yue et al. (2011) and in the operational TEC processing for Swarm (DISC, 2017; Noja et al., 2013).

2.2. Electron Density From KBR

The procedure to approximate inter-satellite electron density from KBR measurements is essentially identical to the methods applied for TEC estimation. As is the case for the GPS receiver, the KBR utilizes two carrier frequencies, K- and Ka-Band (24 and 32 GHz). The KBR observation files as provided by Jet Propulsion Laboratory (JPL) (JPL, 2018; Yuan, 2018) contain the ionospheric phase advance for Ka frequency $Iono_{corr}$. The relative horizontal TEC *rTEC* between the satellite pair can thus be derived as

$$rTEC = \left(Iono_{corr} \cdot f_{Ka}^2\right) \cdot 40.3 \frac{\mathrm{m}^3}{\mathrm{s}^2} \tag{11}$$

The relatively small distance between the satellite pair of only 200 km allows approximating the relative electron density *rNe* as

$$rNe = rTEC/d, \tag{12}$$

where d is the inter-satellite distance (Xiong et al., 2010, 2015). An unknown offset needs to be estimated to obtain the absolute electron density. This offset is assumed to be constant as long as no phase break occurs. In contrast to GPS no absolute measurement is available. Consequently, external input is required. In this work, the external reference is provided by the IRI-2016 model (Bilitza et al., 2017) using the default NeQuick topside. Radar calibration as carried out in Xiong et al. (2015) is not used since the number of conjunctions is very limited and many arcs would have to remain uncalibrated.

3. Data

The TEC processing is based on the GPS observation files in RINEX format. The CHAMP, GRACE and GRACE-FO GPS data have a sampling interval of 10 s. Furthermore, orbit information for both the LEO satellite and the GPS satellites are required. For the LEO missions considered, the most up-to-date versions of the RINEX files are used (isdcftp.gfz-potsdam.de). For CHAMP this implies several changes in the RINEX baseline (i.e., different RINEX processor versions, which is visible in the amount of screened data). The orbits of the LEO satellites are Level 1B GNV for GRACE and GRACE-FO provided by JPL and the rapid science orbits provided by GFZ for CHAMP. The GPS orbits are taken from the Center for Orbit Determination in Europe (CODE) where also the P1-P2 differential code biases for the GPS satellites are provided (ftp.aiub.unibe.ch) (Dach et al., 2020). KBR observation files for GRACE and GRACE-FO are taken from isdcftp.gfz-potsdam.de. The IRI-2016 model and coefficient files are taken from irimodel.org, and radar observation files are collected from the madrigal database http://cedar.openmadrigal.org/.

Multiple preprocessing and screening steps are applied to the GPS and KBR data. The GPS RINEX files are screened for outliers and cycle slips. Outliers, cycle slips, and phase breaks are detected using the Melbourne-Wuebbena linear combination. In case, the deviation from the iterative mean exceeds a fixed σ of 43 cm (equivalent to half a cycle in the Melbourne-Wuebbena linear combination), the arc is split. Furthermore, the data is screened for low Signal to Noise Ratio (SNR) values. Those are translated to carrier noise density for consistency to Swarm and in case its value is lower than 23 dB-Hz the observation is rejected, since the signal quality is assumed to be degraded. The BlackJack onboard CHAMP and GRACE (NASA, 2001) and TriRo-GNSS onboard GRACE-FO (BlackJack heritage) provide LA, L1, and L2 as phase measurements, where LA is L1 tracked on the CA code, L1 refers to the encrypted P(Y)-code tracking and L2 is also tracked on the encrypted P(Y) code on the second frequency. LA can be assumed to have a smaller standard deviation than L1 (Montenbruck & Kroes, 2003) and is thus used instead of L1. Furthermore, near-field multi-path maps are generated on a daily basis as explained earlier. To account for tracking issues, as they occur during flex power active periods (Steigenberger et al., 2018, 2020) onboard GRACE-FO, an additional relative slant TEC screening is applied. For each GPS Pseudo Random Noise (PRN) number with flex power capability (Block IIR-M and IIF) the median relative slant TEC for each connected phase arc is compared. In case an arc has a significantly different median (>50 TECU), the arc is rejected. In consequence code leveled TEC cannot be provided for flex-power

active periods for GRACE-FO for Block IIR-M and IIF GPS satellites if their power redistribution causes code tracking issues.

In the case of KBR data, the data is screened for phase breaks, gaps, and jumps. For GRACE-FO also small jumps at the inter-day boundary were observed, which are corrected by using two extrapolated linear polynomials fitted on the last five observations of the first arc and the first five observations of the second arc. The mean offset is removed afterward. Furthermore, the time series are screened for oscillations and outliers, especially at the start or end of an arc. Arcs are also rejected, if their correlation to IRI derived values is poor (<0.6 (Pearson)) or if the number of observations in one arc is less than 60 points.

4. Results and Validation

4.1. TEC

For all three satellite missions the amount of GPS data used for TEC processing is between 75% and 90% for most of the mission duration (see Figure 4). Several jumps in the performance are visible, especially for CHAMP, GRACE 1, and GRACE-FO 1 and 2. This is primarily caused by the occultation antenna for CHAMP and GRACE 1, which can cause fluctuations in code measurements and therefore lead to a more stringent screening. For GRACE-FO the first step on 14 February 2020 coincides with the activation of Flex Power for the block IIR-M and block IIF GPS satellites. The second large step is caused by receiver updates performed in May 2021 on GRACE-FO 1 and in July 2021 on GRACE-FO 2. In order to improve the tracking performance, the elevation mask of 10° was removed leading to a larger amount of observations in the RINEX files. However, the low elevation observations are affected by a larger code noise and typically weaker SNR, which causes the observations to be rejected in the TEC processing. The drop of the ratio of accepted observations can be seen in Figure 4. If all observations of a single PRN are rejected in the daily processing, it is typically caused by the corresponding PRN missing the orbit files. The reasons are usually maneuvers or the PRN labeled as unhealthy.

The daily TEC maximum observed by CHAMP and GRACE is correlated to averaged F10.7 Index (Figure 5, both as 81-day mean, mean solar flux ranging from 60 sfu to 225 sfu and TEC values up to 170 TECU. During geomagnetic storms the TEC values can even exceed 300 TECU). The correlation coefficients are 0.93 for CHAMP and 0.81/0.82 for GRACE (A/B). For GRACE-FO the correlation is not as well pronounced (0.74/0.71), this is largely due to the short time span of observations and the solar minimum with mean solar flux values ranging from 65 to 85 sfu and thus no significant variation. The maximum TEC values are below 35 TECU. Minimum TEC values scatter around 0 TECU. The scatter is largely caused by the leveling uncertainties. The leveling RMS is in the range of 3 TECU (about 2 TECU due to code noise and 1 TECU caused by the receiver bias estimation). For the differential code bias of the receiver, an oscillation of about 2 TECU is visible for CHAMP. The period is close to 4 months, which indicated a local time and temperature dependency. Nearly identical oscillations are visible for GRACE, which is not unexpected since the GPS receiver and satellite body are nearly identical to CHAMP. For GRACE-FO no such oscillation is observed, which might be related to the low solar flux levels during the presented period, or due to updates in the receiver hardware compared to GRACE/CHAMP. GRACE-FO 2 shows a large jump in the receiver bias in 2018. This jump coincides with the switch of the onboard processing unit in 2018 (JPL, 2020) and can be assumed to be hardware related.

To evaluate the consistency of the derived TEC values between CHAMP, GRACE, and GRACE-FO with Swarm we make use of satellite conjunctions. CHAMP overlaps with GRACE, GRACE with Swarm serving as a link, and Swarm with GRACE-FO. Using these overlaps the entire time series can be made inter-comparable. A conjunction is identified, if the satellites are within 2° of latitude and longitude and the timestamp is within half the sampling interval (10 s for CHAMP, GRACE, and GRACE-FO, and 1 s for Swarm). The total number of conjunctions is 1868/1872 for CHAMP and GRACE-A/B, 601/836 for Swarm B and GRACE-A/B and 787/762 for Swarm B and GRACE-FO 1/2. Swarm A and Swarm C are not shown since the number of conjunction with GRACE(-FO) is lower compared to Swarm B. Vertical TEC is considered and it is required that the elevation of the corresponding mapped slant TEC is larger than 70° to avoid mapping uncertainties. For the differences only identical PRN were considered. To account for the altitude difference between the satellites, vertical TEC from numerical integration of the electron density taken from the IRI-2016 model with default NeQuick topside is used to compensate. A selection of the results is displayed in Figure 6. A striking result is that the offset after IRI correction is nearly 0 (0.1–0.3 TECU), with a variance of less than 2.5 TECU. This variance is largest, in the

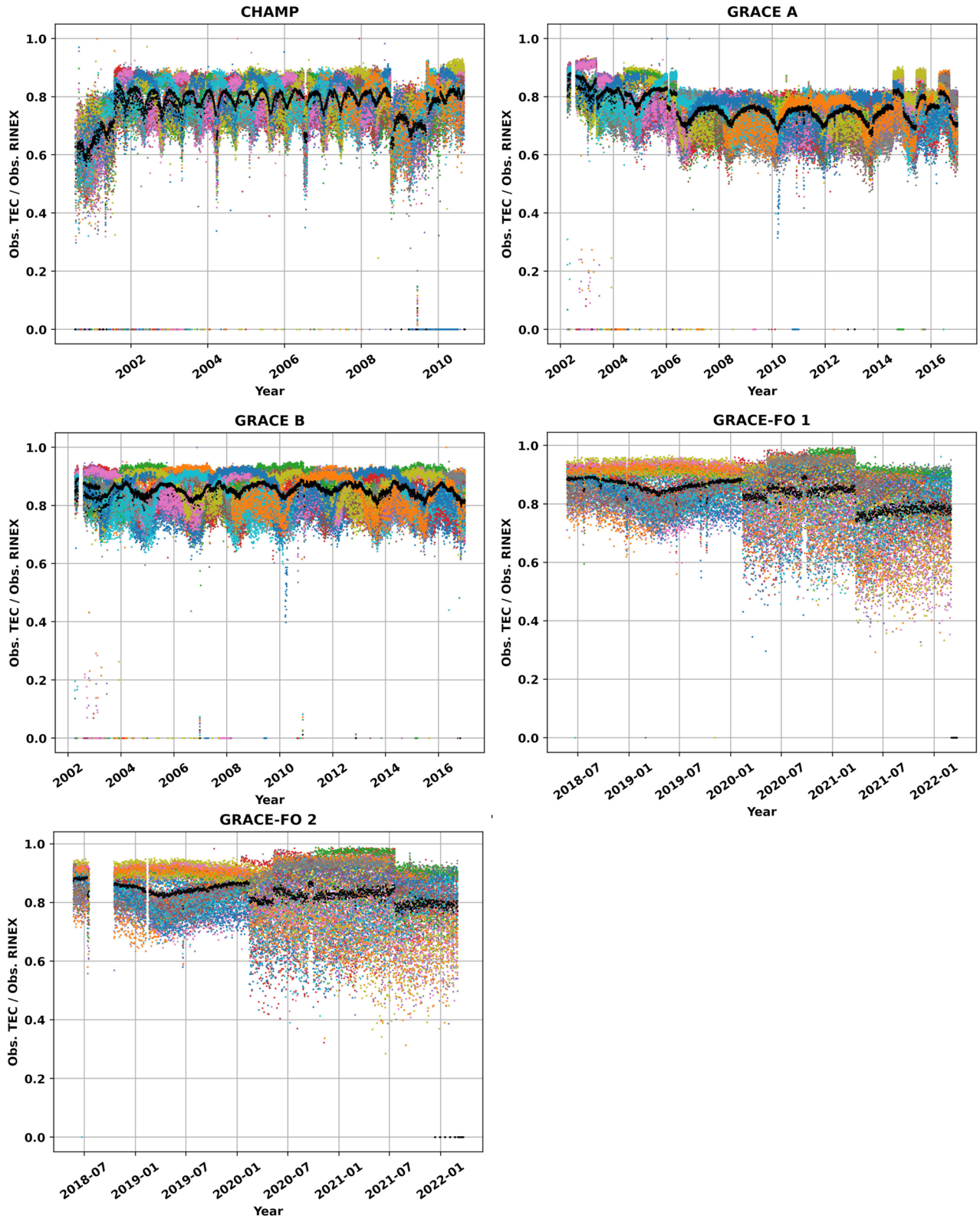

Figure 4. Percentage of Global Positioning System data used for Total Electron Content processing for all five satellites.

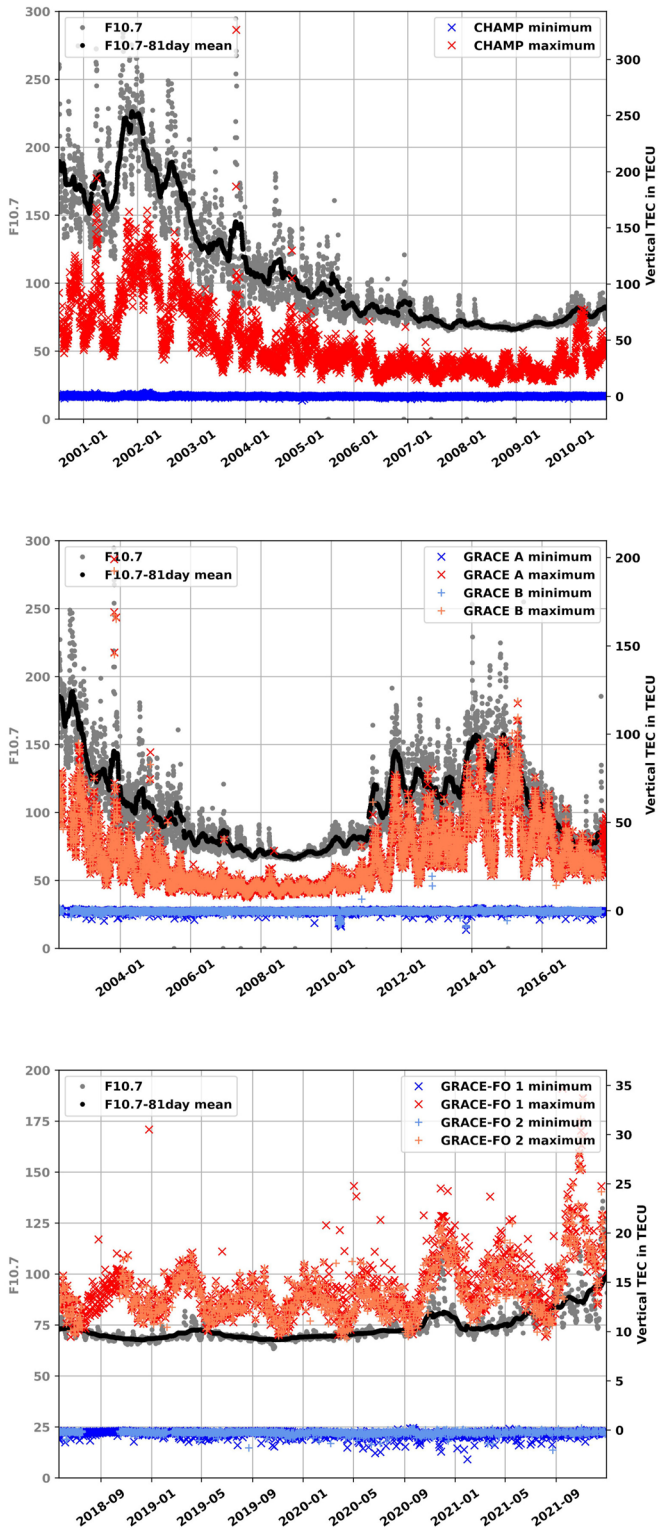

Figure 5. Minimum and maximum total electron content values for the different missions together with the F10.7 Index (left), estimated P1–P2 receiver bias in TECU (right).

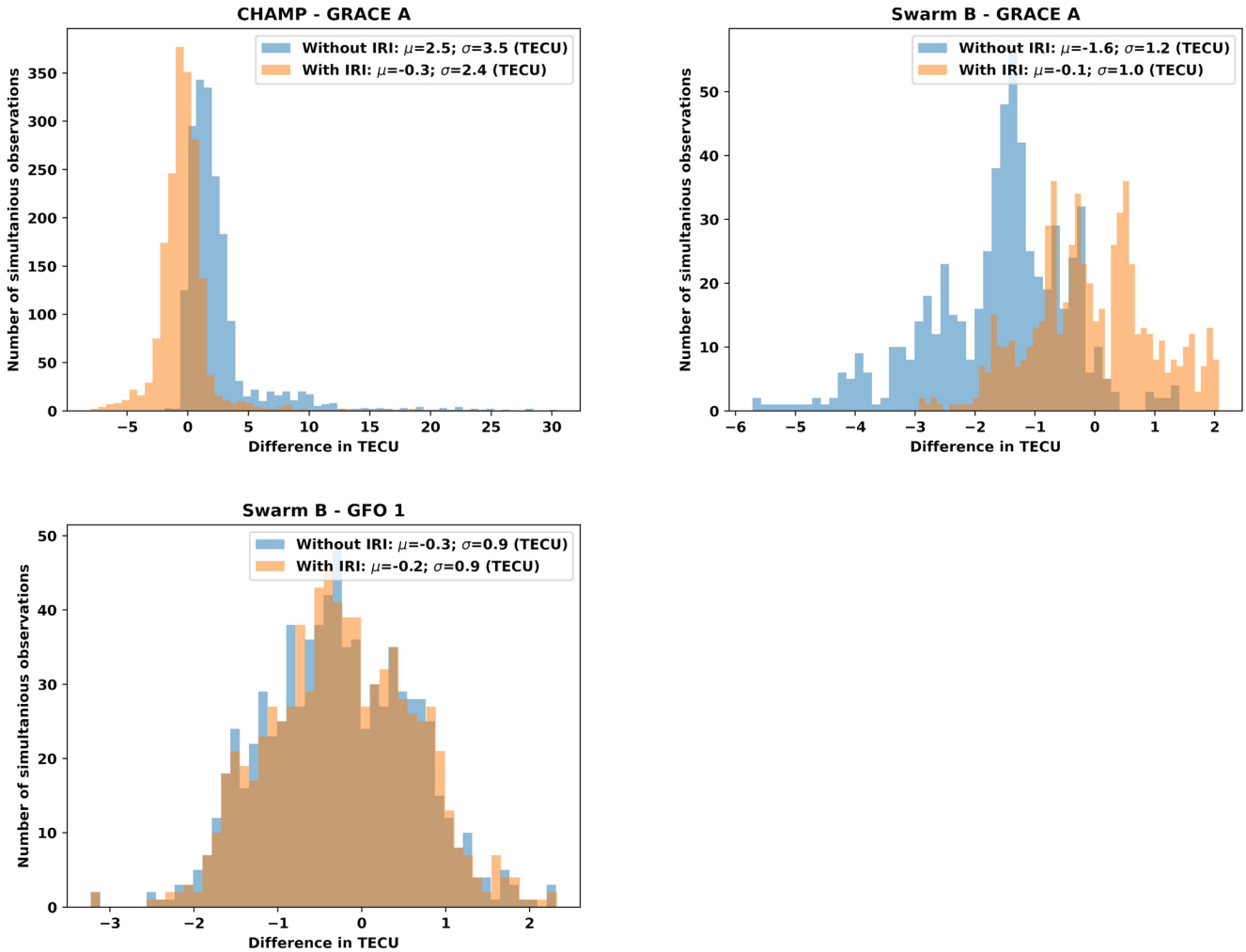

Figure 6. Histogram of vertical total electron content differences before and after compensating for the altitudinal difference using IRI-2016.

case of the CHAMP/GRACE comparison, which have an altitudinal difference of nearly 135 km. Swarm B and GRACE-FO are at nearly identical altitudes. Here the standard deviation is less than 1 TECU proving an excellent agreement between the data sets.

4.2. KBR

The electron density derived from KBR measurements is validated using the IRI-2016 model, ground-based radar observations and conjunctions with Swarm B. The IRI-2016 model allows for a global comparison, whereas radar and satellite conjunctions are sparse and only available for limited time spans and locations. However the comparison to IRI-2016 is not independent since IRI-2016 was used for the absolute calibration. Swarm B Langmuir probe measurements and radar observation are independent and are consequently a good measure of the absolute agreement.

4.2.1. KBR-IRI

A first validation is to evaluate the differences between the KBR derived electron density and the IRI-2016 model estimates. This validation is not entirely independent, since the IRI-2016 model together with the default NeQuick topside is used for calibration of the electron density. However, the climatology provided by IRI should be reproduced in the electron density observations. Apart from the default NeQuick topside we also use the cor2 model (Bilitza & Xiong, 2021). This model includes an F10.7 based correction based on CHAMP and Swarm Langmuir probe measurements and a previous data set of GRACE-KBR electron density observations and can be expected to better represent the topside. The initial topside model of IRI, on which the cor2 model is based, is constructed using

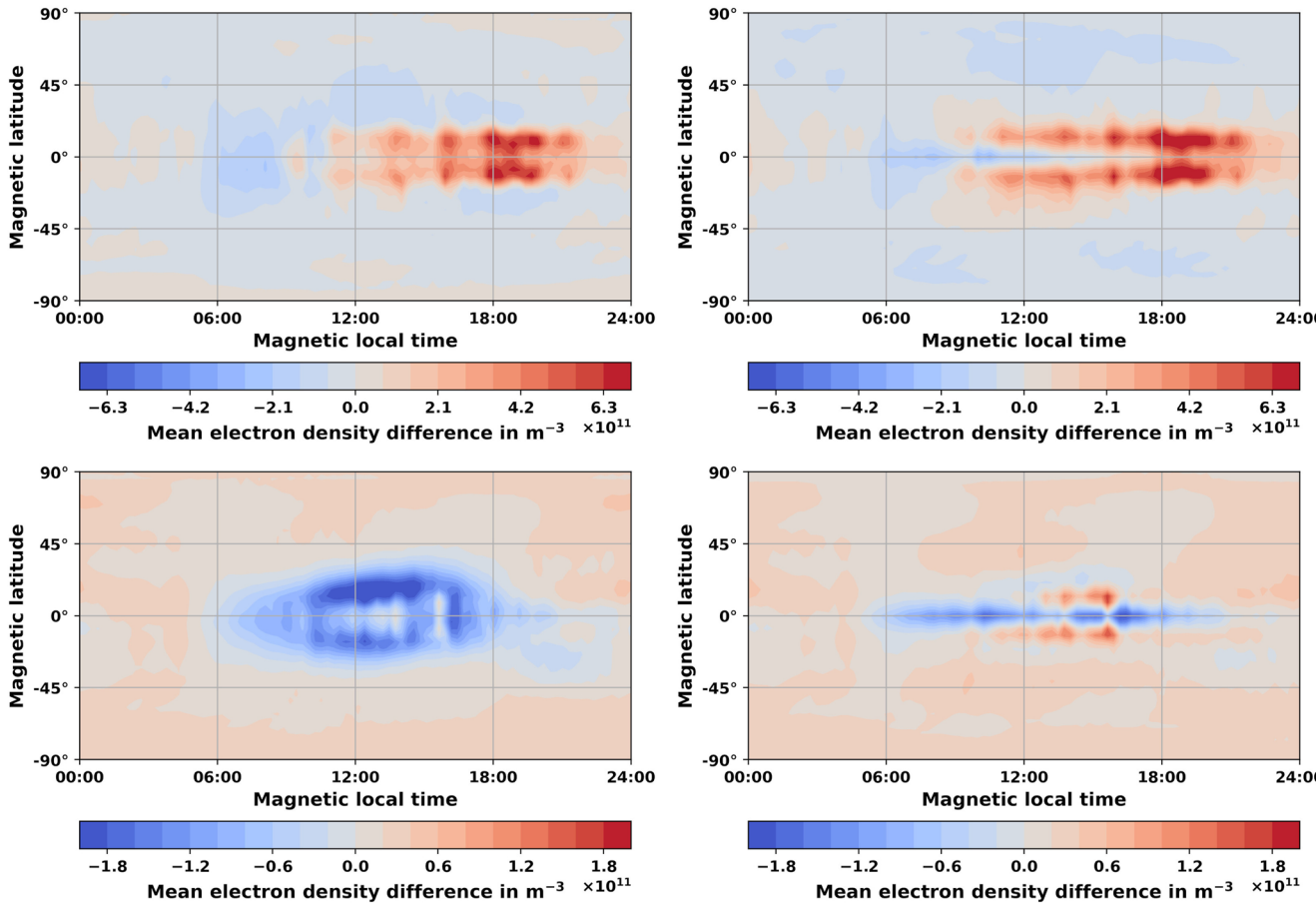

Figure 7. Differences between the GRACE-KBR electron density observations and the IRI-2016 values using the default NeQuick topside (left) and the updated cor2 version (right). Top: Solar maximum condition (2003), bottom: Solar minimum conditions (2008). Positive values: Measured electron density exceeds IRI-2016 electron densities.

topside sounders. The differences between GRACE-KBR and the IRI values binned in geomagnetic latitude and local time are displayed in Figure 7. Since the absolute offset for each arc is zero because of the calibration, relative changes are considered. The accuracy is therefore limited by the (relative) KBR accuracy and the orbit information and can be assumed to be better than 10^9 m^{-3}. For solar maximum conditions as they were present in 2003 one may see, that IRI is underestimating the equatorial ionization anomaly for both, the NeQuick and the cor2 topside model. In the case of the cor2 model, the areas with overestimation are larger, and even the peak is larger compared to NeQuick. For solar minimum conditions as they are observed in 2008, one may see overestimation in the NeQuick topside on large areas between 11 and 17 LT and ±20° magnetic latitude. This overestimation is constrained to a small band near the geomagnetic equator for the cor2 model. Near 15 LT there is however a relatively strong overestimation compared to NeQuick adjacent to the equatorial band. In general, one may conclude, that a good agreement between the model and the KBR measurements is achieved outside the equatorial ionization anomaly, with mean electron density differences in the order of 10^{11} m^{-3}. Furthermore, it should be noted, that the earlier GRACE-KBR electron density data set spans several years of solar minimum conditions, but only a few years of solar maximum conditions.

4.2.2. KBR-Swarm B Langmuir Probes

From September 2019 until the end of December 2019 GRACE-FO and Swarm B were on counter-rotating orbits with less than 20 km altitudinal difference. As Swarm B is equipped with LP to directly measure the ambient electron density, these conjunctions are suited for validation of the electron density obtained by the GRACE-FO KBR. In this comparison the electron density measured by Swarm B is chosen as a reference to compare the KBR results. It should be noted, that Xiong et al. (2022) found that the Swarm LP overestimate the topside plasma density during the solar

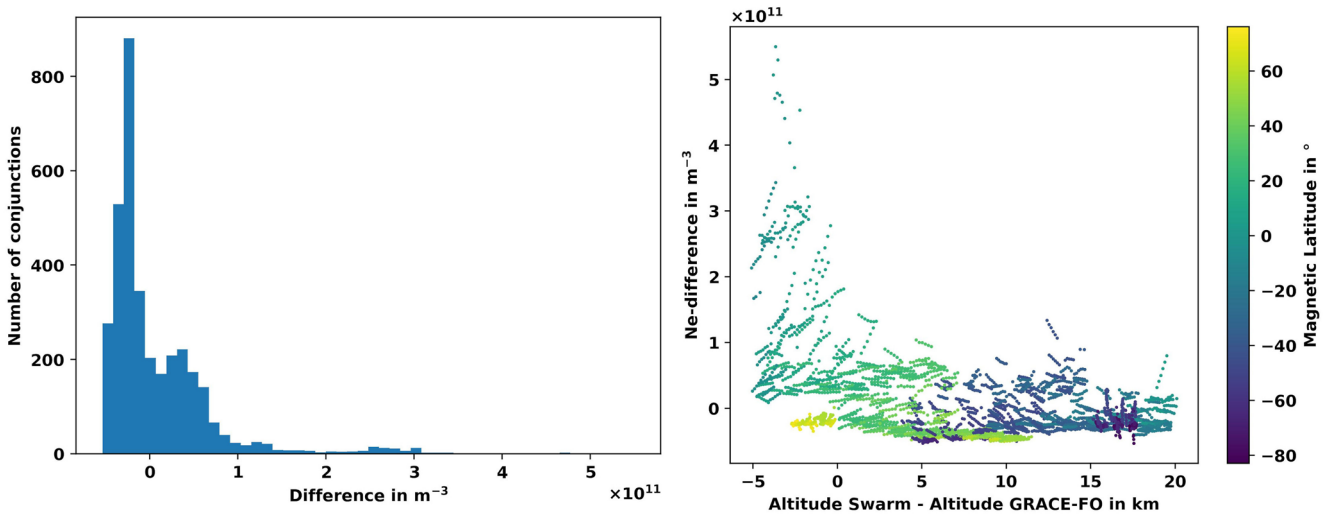

Figure 8. Histogram of electron density differences at GRACE-FO—Swarm B conjunctions (left), and color coded scatter plot showing the difference with respect to geomagnetic latitude and altitude difference.

minimum, as in the algorithm of LP, the plasma has been assumed to be purely O+, which is not the case in solar minimum years at Swarm altitude. The conjunction criteria require the points of measurements (geometrical center of GRACE-FO 1 and GRACE-FO 2, and location of Swarm B) to be within two degrees of longitude and two degrees in latitude. The altitude difference is usually found to be within 20 km. The most up-to-date corrected Swarm B electron density data set labeled as baseline 0601 is used containing the corrected values as described in Lomidze et al. (2018), where external observations from radar station and satellite based radio occultation were used to calibrate Swarm electron densities. In total 3,463 conjunctions could be used. The mean offset μ between the KBR derived electron density and the electron density measured by Swarm is 0.8×10^{10} m^{-3}, whereas the standard deviation σ is 6.4×10^{10} m^{-3}, which means, that the electron density measured at the Swarm LP is larger. These values coincide with the values of the inter-calibration of GRACE-KBR in Smirnov et al. (2021) where an earlier GRACE-KBR electron density data set was used (Xiong et al., 2015). Here the offset compared to COSMIC was - 1.8×10^{10} m^{-3} (GRACE-KBR minus COSMIC electron density) with a standard deviation of 6.3×10^{10} m^{-3}. Which indicated an overestimation of the electron density at the Swarm LP It may be seen that the vast majority of the offsets are close to zero (see Figure 8). Larger offsets of a few 10^{11} m^{-3} are observed which originate from larger measurements of the Swarm LP. In the scatter plot on the right side, it may be seen, that these large values occur if Swarm is a few kilometers below GRACE and in the equatorial regions. In middle and high magnetic latitude regions the differences are much lower, however, the background electron density can also be expected to be much lower resulting in less significant differences.

Table 1
Coordinates of the Radar or Receiver Stations Used for Validation

Station	Lat	Lon	mlat[a]	mlon[a]
ARO	18.3	293.3	27.2	10.5
JRO	−12.0	283.1	0.2	−4.4
MLH	42.6	288.5	51.8	7.6
REB	74.7	265.1	82.6	−35.7
EISCAT Kiruna	67.9	20.4	64.7	102.1
EISCAT Tromso	69.6	19.2	66.5	102.3
EISCAT Sodankylä	67.4	26.6	64.0	106.8
EISCAT Svalbard	78.1	16.0	75.2	110.1
PFA	65.1	212.6	65.3	−93.7

Note. In Resolute Bay the two radars are co-located. Thus only one coordinate set is given.
[a]Reference date 1 January 2010.

4.2.3. KBR-Radar

An essential tool to measure ionospheric key parameters such as the topside electron density is incoherent scatter radars. For evaluating the electron density measured by radar and measured by GRACE(-FO) KBR we use data provided by the Arecibo Radar Observatory (ARO), Jicarmarca Radio Observatory (JRO), Millstone Hill, Resolute Bay (REB), European Incoherent Scatter Scientific Association (EISCAT) and Poker Flat Radar (PFA). Unfortunately, some of the radar stations are in high magnetic latitudes (see Table 1). This causes irregular profiles and large observational errors for these radar stations and thus a large scatter at GRACE(-FO) altitude. The radar observations are filtered using the following criteria. First, only data is considered, that satisfy conjunction criteria with GRACE(-FO). Those conjunction criteria are:

- Satellite within 5° longitude of the Radar station.
- Satellite within 5° latitude of the Radar station.
- Maximum 15 min between radar measurement and overflight.

Table 2
Number of Usable Conjunctions With the Radar Station for Gravity Recovery and Climate Experiment and GRACE-FO (Until End 2021)

Sat	ARO	JRO	MLH	REB	EISCAT	PFA
GRACE	131	82	390	247	988	1,215
GRACE-FO	0	2	19	0	13	2

- At least one observation within 20 km of satellite altitude.
- Radar observations below and above satellite altitude.

Every single profile is screened for smoothness using a polynomial fit. If the relative error is large (Root Mean Squared Error (RMS) >0.6 times the interpolated electron density at satellite altitude) the whole profile is rejected. All observations satisfying these criteria are selected, screened for large observational errors (electron density lower than $5 \times dNe$, where dNe is the observational error for the electron density in the radar observation file), if less than four points remain the profile is rejected. Smoothing is applied using the least squares fit of a quadratic polynomial on log 10(Ne) starting from 100 km below the satellite altitude up to 100 km above satellite altitude. The least squares fit is weighted with the inverse of the observational error given in the radar observation files. Points outside the three sigma range are rejected and the smoothing is repeated on the cleaned data set. Eventually, the fitted polynomial is evaluated at GRACE(-FO) altitude, which is used as a reference value.

The smoothest profiles are obtained from the ARO and JRO stations. These are in low latitude regions, where the ionospheric profile also has significant values for higher altitudes. For high latitude stations, such as EISCAT and REB the errors regarding the polynomial fit on the radar observations are much larger and may lead to unrealistic large values. To ensure a good quality of fit, again the RMS is compared. If the RMS of fit is larger than the value of the fitted curve at satellite altitude, the profile is not used.

All these restrictions lead to a very limited number of usable conjunction, especially for GRACE-FO (see Table 2). Consequently the histogram and scatter plots are only shown for GRACE. In Figure 9 one may see the distribution of the differences between the derived GRACE electron density and the radar electron density. For all radar stations, a positive offset is visible within the range of up to 7×10^{10} m^{-3}. This is an indicator that the IRI model, and thus the IRI calibrated data, is underestimating the ambient electron density. For all radar stations the standard deviation is near 10^{11} m^{-3}. The largest standard deviation is observed for Jicarmarca where also the largest electron density is present. One can also see in Figure 7 that the stations in equatorial regions are prone to have the largest deviations in the calibration. For these stations, differences in local time that are not accounted for may become significant (Rother et al., 2010; Xiong et al., 2015).

The agreement between the GRACE electron density and the radar values is best for Arecibo and Jicarmarca (both 0.96, see Figure 10). The observed scale parameter of less than 1 again indicates that the GRACE electron density relying on the IRI model is underestimated. For near-equatorial stations, this is due to the amplitude of the electron density near solar maximum. Already in the previous comparison with IRI, see Figure 7, it was found that in equatorial regions the observed electron density is higher than the electron densities calculated by IRI, even though the arc-wise mean offset is removed during the calibration procedure. For REB and EISCAT the correlation is poor, which is partially caused by the limitations of the radar observations due to the very low electron densities, and because the assumption for the exponential decay does not hold because of the irregularity of ionospheric profiles at higher altitudes in high latitude regions.

The conclusion which can be drawn from the comparison to radar observation, especially the scale factor, is that an underestimation of 10%–15% in electron density may be caused by the IRI calibration.

5. Conclusions

The already existing database of LEO GPS TEC and electron density observations has proven its potential to understand and describe the topside ionosphere. The newly processed data obtained from CHAMP, GRACE, and GRACE-FO extends the already available data sets from SWARM and GOCE and allows to cover two full solar cycles without gaps by LEO GPS TEC data. A continuous time series of electron density data is also provided by GRACE, Swarm, and GRACE-FO. It is shown, that the routinely processed Swarm and the new (CHAMP, GRACE(-FO)) TEC data sets are highly consistent and that their accuracy matches the theoretical thresholds of the processing scheme. Compared to radar, Swarm B and IRI, the high quality and accuracy of the KBR electron density are also confirmed. Nevertheless, the limit for the electron density is the calibration, which has been determined using an external source.

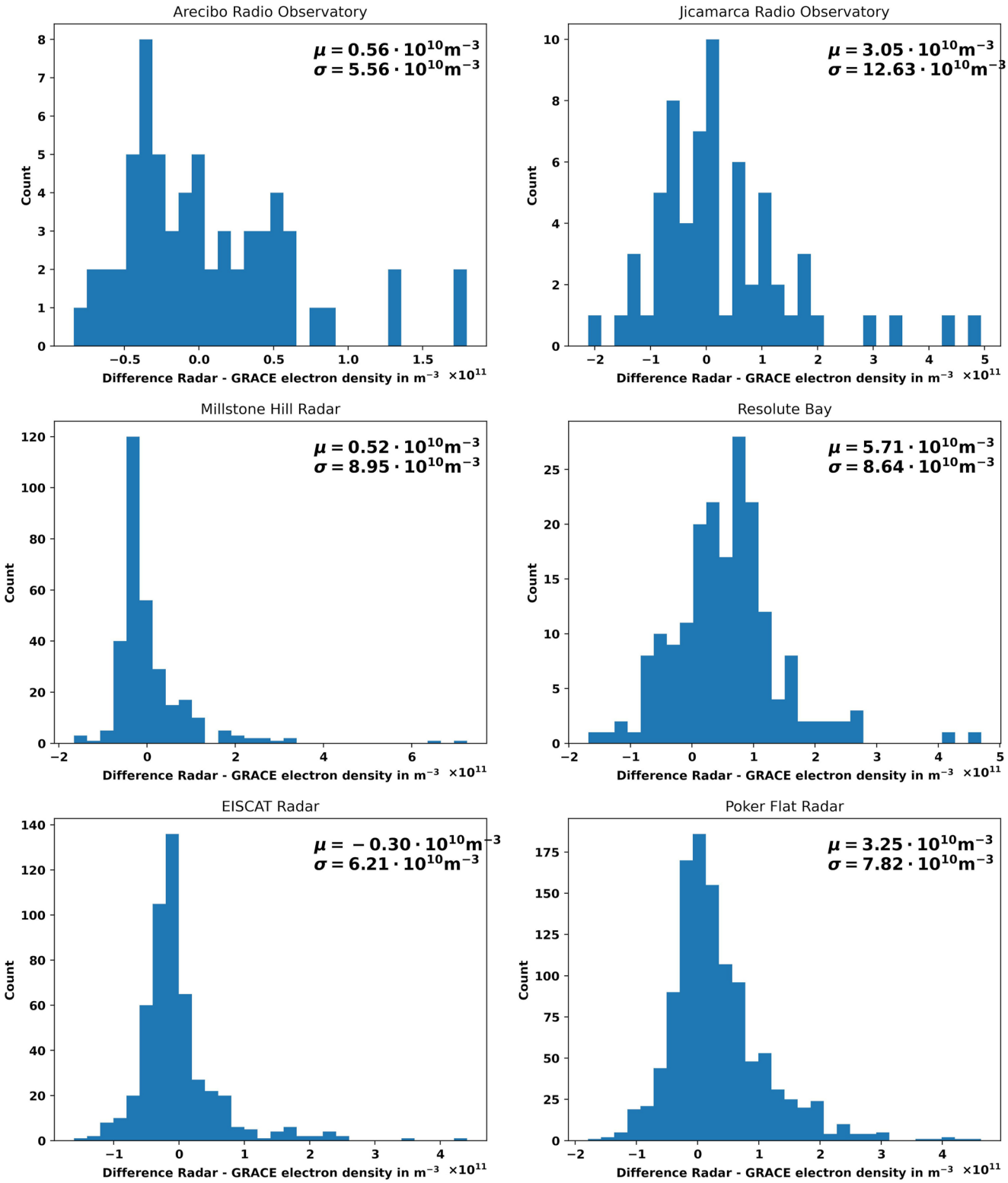

Figure 9. Differences between the International Reference Ionosphere calibrated data set and the radar based electron density for Gravity Recovery And Climate Experiment.

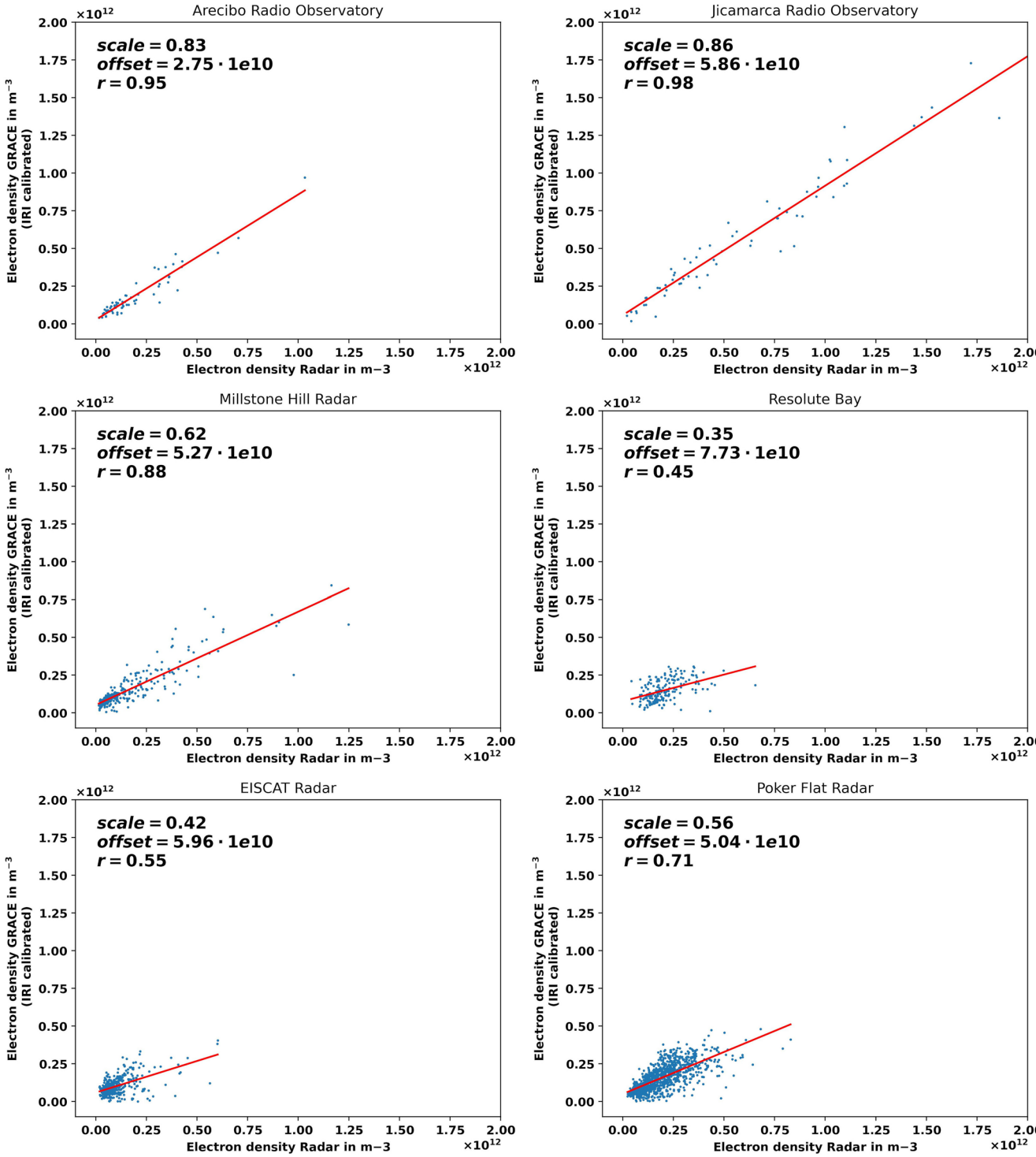

Figure 10. Radar electron density and Gravity Recovery And Climate Experiment International Reference Ionosphere calibrated electron density together with a linear fit and the correlation coefficient *r*.

Data Availability Statement

RINEX observation files for CHAMP, GRACE and GRACE-FO as well as the science orbits are available at isdcftp.gfz-potsdam.de. The GPS orbits and differential code biases are provided by the Center for Orbit Determination in Europe (CODE) ftp.aiub.unibe.ch. KBR observation Files for GRACE and GRACE-FO are available

at isdcftp.gfz-potsdam.de. The IRI-2016 model and coefficient files are taken from irimodel.org, and Radar observation files are available at the madrigal database http://cedar.openmadrigal.org/.
The resulting TEC and electron density files are made available at isdcftp.gfz-potsdam.de/grace/IONOSPHERE/, isdcftp.gfz-potsdam.de/grace-fo/IONOSPHERE/, isdcftp.gfz-potsdam.de/champ/IONOSPHERE/, and via ESA https://swarm-diss.eo.esa.int/.

Acknowledgments
This work is funded the European Space Agency (ESA) through Technical University of Denmark (DTU)—ITT 3.3 Extending Swarm TEC products with data from other LEO satellites (subcontract number SW-CO-DTU-GS-126). Open Access funding enabled and organized by Projekt DEAL.

References

Bilitza, D. (2018). IRI the International Standard for the Ionosphere. *Advances in Radio Science*, *16*, 1–11. https://doi.org/10.5194/ars-16-1-2018
Bilitza, D., Altadill, D., Truhlik, V., Shubin, V., Galkin, I., Reinisch, B., & Huang, X. (2017). International Reference Ionosphere 2016: From ionospheric climate to real-time weather predictions. *Space Weather*, *15*(2), 418–429. https://doi.org/10.1002/2016SW001593
Bilitza, D., & Williamson, R. (2000). Towards a better representation of the IRI topside based on ISIS and Alouette data. *Advances in Space Research*, *25*(1), 149–152. https://doi.org/10.1016/S0273-1177(99)00912-6
Bilitza, D., & Xiong, C. (2021). A solar activity correction term for the IRI topside electron density model. *Advances in Space Research*, *68*(5), 2124–2137. https://doi.org/10.1016/j.asr.2020.11.012
Case, L., Kruizinga, G., & Wu, S. (2010). GRACE Level 1B Data Product User Handbook. Retrieved from https://podaac-tools.jpl.nasa.gov/drive/files/allData/grace/docs/Handbook_1B_v1.3.pdf
Dach, R., Lutz, S., Walser, P., & Fridez, P. (Eds.). (2015). *Bernese GNSS Software Version 5.2 user manual*. Astronomical Institute, University of Bern, Bern Open Publishing.
Dach, R., Schaer, S., Arnold, D., Kalarus, M. S., Prange, L., Stebler, P., et al. (2020). *CODE final product series for the IGS*. Published by Astronomical Institute, University of Bern. Retrieved from http://www.aiub.unibe.ch/download/CODE, https://doi.org/10.7892/boris.75876.4
DISC. (2017). *Swarm Level 2 TEC product description (Technical Report)*. ESA, BGS, DTU, DUT, GFZ, ETH, IPGP, IRF, Leti, UoC, VZLU.
Drinkwater, M., Haagmans, R., Muzi, D., Popescu, A., Floberghagen, R., Kern, M., & Fehringer, M. (2006). The GOCE gravity mission: ESA's first core explorer. In *Proceedings of the 3rd GOCE User Workshop, 6–8 Nov 2006, Frascati, Italy, ESA SP-627* (pp. 1–7).
Foelsche, U., & Kirchengast, G. (2002). A simple "geometric" mapping function for the hydrostatic delay at radio frequencies and assessment of its performance. *Geophysical Research Letters*, *29*(10), 111-1–111-4. https://doi.org/10.1029/2001GL013744
Fritsche, M., Dietrich, R., Knöfel, C., Rülke, A., Vey, S., Rothacher, M., & Steigenberger, P. (2005). Impact of higher-order ionospheric terms on GPS estimates. *Geophysical Research Letters*, *32*(23), L23311. https://doi.org/10.1029/2005GL024342
JPL. (2018). GRACE-FO resumes data collection. Retrieved from https://gracefo.jpl.nasa.gov/news/140/grace-fo-resumes-data-collection/
JPL. (2020). Grace-FO mission overview. Retrieved from https://gracefo.jpl.nasa.gov/mission/overview/
Kervalishvili, G., Xiong, C., Rauberg, J., Stolle, C., van den IJssel, J., & Schreiter, L. (2019). Total Electron Content (TEC) and the Rate Of change of TEC Index (ROTI) derived from ESA's Low Earth Orbit (LEO) mission observations. *Living Planet Symposium (Milan, Italy 2019)*. Retrieved from https://gfzpublic.gfz-potsdam.de/pubman/item/item_5003001
Lei, J., Wang, W., Burns, A. G., Yue, X., Dou, X., Luan, X., et al. (2014). New aspects of the ionospheric response to the October 2003 superstorms from multiple-satellite observations. *Journal of Geophysical Research: Space Physics*, *119*(3), 2298–2317. https://doi.org/10.1002/2013JA019575
Lomidze, L., Knudsen, D. J., Burchill, J., Kouznetsov, A., & Buchert, S. C. (2018). Calibration and validation of Swarm plasma densities and electron temperatures using ground-based radars and satellite radio occultation measurements. *Radio Science*, *53*(1), 15–36. https://doi.org/10.1002/2017RS006415
Montenbruck, O., & Kroes, R. (2003). In-flight performance analysis of the CHAMP BlackJack GPS Receiver. *GPS Solutions*, *7*(2), 74–86. https://doi.org/10.1007/s10291-003-0055-5
NASA. (2001). BlackJack GPS receiver. *NASA Tech Briefs NPO-20891*. Retrieved from http://www.nasatech.com/Briefs/June01/NPO20891.html
Noja, M., Stolle, C., Park, J., & Lühr, H. (2013). Long-term analysis of ionospheric polar patches based on CHAMP TEC data. *Radio Science*, *48*(3), 289–301. https://doi.org/10.1002/rds.20033
Reigber, C., Schwintzer, P., & Lühr, H. (1999). The CHAMP geopotential mission. *Bollettino di Geofisica Teorica ed Applicata*, *40*, 285–289.
Rother, M., Schlegel, K., Lühr, H., & Cooke, D. (2010). Validation of CHAMP electron temperature measurements by incoherent scatter radar data. *Radio Science*, *45*(6). https://doi.org/10.1029/2010RS004445
Schaer, S. (2011). Activities of IGS bias and calibration working group. In M. Meindl, R. Dach, & Y. Jean (Eds.), *IGS Technical Report 2011*.
Smirnov, A., Shprits, Y., Zhelavskaya, I., Lühr, H., Xiong, C., Goss, A., et al. (2021). Intercalibration of the plasma density measurements in Earth's topside ionosphere. *Journal of Geophysical Research: Space Physics*, *126*(10), e2021JA029334. https://doi.org/10.1029/2021JA029334
Steigenberger, P., Thölert, S., Esenbuga, O. G., Hauschild, A., & Montenbruck, O. (2020). The new flex power mode: From GPS IIR-M and IIF Satellites with extended coverage area. *Inside GNSS*. Retrieved from https://insidegnss.com/the-new-flex-power-mode-from-gps-iir-m-and-iif-satellites-with-extended-coverage-area/
Steigenberger, P., Thölert, S., & Montenbruck, O. (2018). Flex power on GPS block IIR-M and IIF. *GPS Solutions*, *23*(1), 1521–1886. https://doi.org/10.1007/s10291-018-0797-8
Tapley, B. D., Bettadpur, S., Ries, J. C., Thompson, P. F., & Watkins, M. M. (2004). GRACE measurements of mass variability in the Earth system. *Science*, *305*(5683), 503–505. https://doi.org/10.1126/science.1099192
Xiong, C., Jiang, H., Yan, R., Lühr, H., Stolle, C., Yin, F., et al. (2022). Solar flux influence on the in-situ plasma density at topside ionosphere measured by swarm satellites. *Journal of Geophysical Research: Space Physics*, *127*(5), e2022JA030275. https://doi.org/10.1029/2022JA030275
Xiong, C., Lühr, H., Ma, S., & Schlegel, K. (2015). Validation of GRACE electron densities by incoherent scatter radar data and estimation of plasma scale height in the topside ionosphere. *Advances in Space Research*, *55*(8), 2048–2057. https://doi.org/10.1016/j.asr.2014.07.022
Xiong, C., Lühr, H., & Stolle, C. (2021). GRACE electron density derived from the K-band ranging system (KBR). V. 0101. https://doi.org/10.5880/GFZ.2.3.2021.003
Xiong, C., Park, J., Lühr, H., Stolle, C., & Ma, S. Y. (2010). Comparing plasma bubble occurrence rates at CHAMP and GRACE altitudes during high and low solar activity. *Annales Geophysicae*, *28*(9), 1647–1658. https://doi.org/10.5194/angeo-28-1647-2010
Yuan, D. (2018). GRACE 327-744, Gravity Recovery And Climate Experiment, JPL Level-2 Processing Standards Document. Retrieved from https://podaac-tools.jpl.nasa.gov/drive/files/GeodeticsGravity/grace/docs/L2-JPL_ProcStds_v6.0.pdf
Yue, X., Schreiner, W. S., Hunt, D. C., Rocken, C., & Kuo, Y.-H. (2011). Quantitative evaluation of the low Earth orbit satellite based slant total electron content determination. *Space Weather*, *9*(9), S09001. https://doi.org/10.1029/2011SW000687